agriculture

MDPI

Article

Dynamic Cutting Performance Test and Parameter Optimization of Longicorn Bionic Blade for Industrial Hemp Harvester

Kunpeng Tian [1,2], Bin Zhang [2], Cheng Shen [2], Haolu Liu [2], Jicheng Huang [2,*] and Aimin Ji [1,*]

[1] College of Mechanical and Electrical Engineering, Hohai University, Changzhou 213022, China
[2] Nanjing Institute of Agricultural Mechanization, Ministry of Agriculture and Rural Affairs, Nanjing 210014, China; xtsset@hotmail.com (B.Z.); shencheng1989@cau.edu.cn (C.S.); liuhaolu@caas.cn (H.L.)
* Correspondence: huangjicheng@caas.cn (J.H.); jiam@hhuc.edu.cn (A.J.)

Abstract: In response to the unclear issue of whether the dynamic cutting performance and structural parameters of an industrial hemp blade, which was developed earlier based on the bionic prototype of the batocera horsfieldi, can be optimized in actual working conditions, this paper analyzes the effective clamping conditions of a reciprocating double-acting cutting blade for stalks and the cutting motion. To investigate the effect of different structural and motion parameters, as well as their interactions, of the bionic blade on cutting energy consumption, bionic blades with different combinations of tooth pitch and tooth angle were designed. A Box–Behnken response surface method with three factors and three levels was used to design an experimental scheme. Utilizing rigid-flexible coupling numerical simulation technology, numerical simulation experiments were conducted to investigate the cutting performance of industrial hemp stalks using the blade. A regression model for cutting energy consumption was established, and variance analysis indicated that tooth angle, speed ratio, and the interaction between tooth angle and speed ratio had an extremely significant effect on the regression model. The primary and secondary orders of factors affecting cutting energy consumption were determined to be: speed ratio > tooth angle > tooth pitch. Through optimization, the optimal parameter combination was found to be a blade tooth pitch of 6.61 mm, a tooth angle of 30°, and a speed ratio of 1.62. Under these conditions, the cutting energy consumption was 3947.99 mJ. The optimized parameters were verified through numerical simulation cutting experiments, and the results showed that the error compared with the optimization results was only 8.16%. This indicates that the optimization results have high credibility and further verifies the reliability of the model. This study can provide a reference for the development of cutting devices for industrial hemp harvesters and the selection of motion parameters.

Keywords: industrial hemp; bionic blade; cutting energy consumption; numerical simulation; parameter optimization

Citation: Tian, K.; Zhang, B.; Shen, C.; Liu, H.; Huang, J.; Ji, A. Dynamic Cutting Performance Test and Parameter Optimization of Longicorn Bionic Blade for Industrial Hemp Harvester. *Agriculture* **2023**, *13*, 1074. https://doi.org/10.3390/agriculture13051074

Academic Editors: Muhammad Sultan, Redmond R. Shamshiri, Md Shamim Ahamed and Muhammad Farooq

Received: 29 April 2023
Revised: 15 May 2023
Accepted: 15 May 2023
Published: 17 May 2023

1. Introduction

Industrial hemp, also known as *Cannabis sativa* L., refers to a non-psychoactive variety of cannabis with a THC (tetrahydrocannabinol) content of less than 0.3% [1–3]. Due to its low THC content, it lacks drug-related value, but its fibers are highly resilient, moisture-absorbent, breathable, antibacterial, and radiation-resistant, so it is widely used in various fields, such as textiles, papermaking, environmental materials, and military equipment [4–7]. In recent years, with the medicinal value of industrial hemp extract cannabidiol (CBD) in anti-tumor, neuroprotection, metabolism, and immune regulation being discovered, more and more countries and regions have announced the legalization of industrial hemp, and the industrial hemp industry is rapidly developing [8,9], gradually becoming a new global industry hotspot [10].

Harvesting is a crucial step in the industrial hemp production process. However, due to the lack of mature harvesting equipment, current industrial hemp harvesting in China

still relies on traditional manual methods, which are labor-intensive, inefficient, and costly, making it difficult to meet the demands of modern hemp production. In recent years, the research and development work of industrial hemp harvesters have been carried out by the author's team [11]. However, due to the lack of specialized cutting blades with high adaptability, the harvester can only use reciprocating blades from traditional rice and corn harvesters. Compared to crops, such as rice, wheat, corn, and flax, industrial hemp plants are taller and sturdier, with tough and strong hemp fiber and hard woody stalks. The traditional blades from rice and wheat harvesters are no longer suitable for the cutting requirements of hemp stalks, which has led to high cutting energy consumption, severe fiber tearing, low stalk cutting rate, and issues, such as fiber wrapping, stalk blockage, and high machine failure rate, during harvesting operations. Therefore, cutting has become a bottleneck issue that urgently needs to be addressed in the field of industrial hemp harvesting [12].

To address the bottleneck issue of poor cutting quality, the author utilized the biomimetic approach in the early stage, taking the batocera horsfieldi, a common pest with excellent biting and cutting performance in hemp fields, as the bio-inspired object. They designed industrial hemp harvester bionic blades based on the structural characteristics of the batocera horsfieldi's mouthpart palates. Comparative experiments were conducted between the bionic blades and conventional rice and wheat harvester blades for single stalk cutting performance. The results showed that compared to conventional blades, the average maximum cutting force and cutting power of the bionic blades were reduced by 7.4% and 8.0%, respectively, and the cutting residues were more even. The bionic blades demonstrated superior cutting performance [12]. However, this study only focuses on the horizontal comparison of cutting performance between two types of blades, bionic and ordinary, and the experimental method only involves single stalk cutting at low speed (loading speed of 25 mm/min) using an electronic universal testing machine. It is still unclear how the dynamic cutting performance of the blades will be in actual operating conditions, and whether the blade structure can be further optimized, which requires further research.

Cutting is a complex process of interaction between rigid blades and flexible stalks, which is difficult to study theoretically. The use of numerical simulation technology can establish a visual virtual cutting environment and provide guidance for the development of cutters [13]. Relevant studies are as follows: Huang H. et al. used Ansys/LS-Dyna to simulate and analyze the sugarcane cutting process, and they determined the maximum stress values and distribution positions of the blade and sugarcane [14]. Qiu M. et al. utilized numerical simulation techniques to investigate the blade motion and stress wave propagation patterns during the sugarcane cutting process, revealing the mechanism of sugarcane cutting [15]. Yang W. et al. simulated the forces acting on the surface of the sugarcane blade and root system using a finite element and SPH coupling method [16]. Xue Z. combined the constitutive model parameters of cassava stem and used ANSYS to carry out numerical simulation analysis of the circular cutter cutting cassava stem, analyzing the stress, deformation, and damage to the cassava stem under different cutter structural parameters, providing reference for the optimization design of the cutter [17]. Meng Y. et al. conducted an explicit dynamic simulation based on Ansys/LS-Dyna on the process of saw cutting mulberry branches, analyzed the interaction process between the saw blade and mulberry branches, and optimized the structural parameters of the saw blade through virtual cutting experiments [18]. Similar research has also been carried out in areas, such as sugarcane topping [19], soybean [20], tomato [21], cotton [22], chrysanthemum stalks [23,24], and wood cutting [25]. The above studies show that numerical simulation methods represented by the finite element method can intuitively and quantitatively analyze the dynamic cutting mechanical properties of the blade on the stalk, and can provide an effective method for the development of low-energy-consumption crop stalk blades.

Considering this, this study will use numerical simulation technology to conduct numerical simulation experiments on blade cutting under different blade structure parameters and motion parameters, in order to determine the optimal parameter combination for

industrial hemp stalk cutting and provide a reference for the development of industrial hemp harvester cutters.

2. Overall Structure and Working Principle of Industrial Hemp Harvester

The industrial hemp harvester is mainly composed of components, such as a divider, a cutting platform frame, a lateral conveying device (with three layers of conveying chains), a cutting device, a longitudinal conveying device, a stalk collection bin, and a chassis. The overall structure is shown in Figure 1, and the cutting device is illustrated in Figure 2.

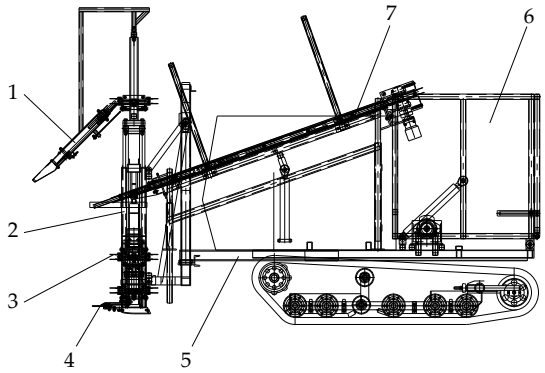

Figure 1. Overall structure and working principle of industrial hemp harvester. 1. Divider; 2. cutting platform frame; 3. lateral conveying device; 4. cutting device; 5. chassis; 6. stalk collection bin; 7. longitudinal conveying device.

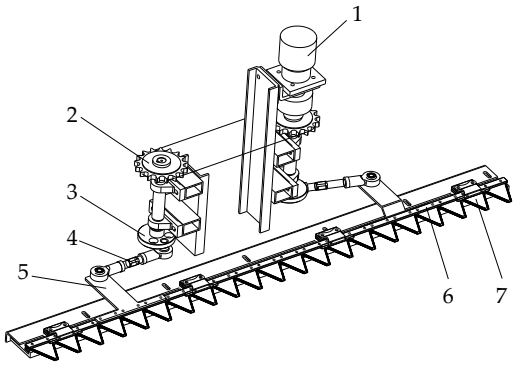

Figure 2. Structure diagram of the cutting device. 1. Hydraulic motor; 2. sprocket drive device; 3. eccentric disc; 4. articulated bearing components; 5. connecting arm; 6. blade-fixing rod; 7. blade.

The working principle is as follows: During operation, the divider separates the intertwined upper part of the hemp stalk and transfers it to the rear lateral conveying device. At the same time, the cutting device located in the lower part of the cutting platform cuts off the bottom part of the hemp stalk. The severed hemp stalk is pushed by the lateral conveying device towards one side of the cutting platform. When the stalk reaches the end of the cutting platform, it turns and enters the longitudinal conveying device. Finally, the longitudinal conveying device transports the hemp stalk to the stalk collection bin. When the stalk collection bin is full, it is manipulated to tilt and unload the collected hemp stalk. The cutting device is driven by a hydraulic motor, and power is transmitted through a sprocket drive to rotate an eccentric disc. The crank-connecting rod mechanism, composed of the left and right eccentric discs and articulated bearing components, converts the rotary motion into linear reciprocating motion, thereby achieving the reciprocating cutting of the blade.

3. Stalk Cutting Theoretical Analysis and Bionic Blade Design

3.1. Analysis of Cutting Force on Reciprocating Double-Acting Blade

For the reciprocating double-acting blade, the premise for ensuring effective cutting is that the blade should be able to firmly clamp the stalk and not slip. The force analysis of the blade when cutting hemp stalks is shown in Figure 3.

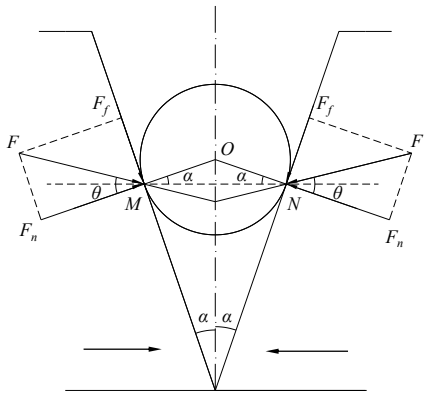

Figure 3. Analysis of cutting force. Note: an arrow indicates the direction of the blade's motion.

When the left and right blades simultaneously move towards the center for cutting, the hemp stalk tends to slide forward due to the squeezing force of the blade. At the contact points M and N between the blades and the stalk, the stalk is subjected to normal compression force F_n and frictional force F_f along the direction of the blade, and the resultant force is F. The angle between the normal force F_n and the resultant force F is the friction angle θ, which can be expressed by the following equation:

$$F_f = F_n \tan\theta \tag{1}$$

According to the force balance condition, the critical equilibrium condition for the stalk to be clamped and not slide is that the magnitude of the resultant force F at the contact points M and N between the blades and the stalk is equal and opposite, and they are on the same line. At this point, the cutting angle α of the blade is equal to the friction angle θ, which indicates that the condition for the stalk to be stably clamped by the blade is that the cutting angle of the blade is less than or equal to the friction angle, i.e.,

$$\alpha \leq \theta \tag{2}$$

The cutting angle α of the reciprocating cutting blade designed in this study is 19° [12]. It is known that the friction angle between the blade and the agricultural crop stalk is generally greater than 34° [26] (p. 913), which means that the blade satisfies the condition of effective clamping and no slippage.

3.2. Cutting Motion Analysis

The reciprocating cutter is driven by a crank-rocker mechanism. Compared with a single-acting cutter, the cutting stroke S of the double-acting blade can be reduced by half after one cutting, that is,

$$S = b/2 = 2r \tag{3}$$

where b is the blade width and r is the crank radius.

The movement of the blade of a reciprocating cutter driven by a crank-link mechanism can be approximated as intermittent motion. The displacement x, velocity v, and

acceleration a of any point on the cutting edge are variable (as shown in Figure 2) and can be expressed by the following equations:

$$\begin{cases} x = -r\cos\omega t \\ v = r\omega\sin\omega t = \omega\sqrt{r^2 - x^2} \\ a = r\omega^2\cos\omega t = -\omega^2 x \end{cases} \quad (4)$$

In the equation, ω represents the angular velocity of the crankshaft, measured in rad/s, and t represents the time elapsed since the crankshaft passed through the left dead point, measured in s.

According to Equation (4), the following formula can be obtained:

$$\frac{v^2}{(r\omega)^2} + \frac{x^2}{r^2} = 1 \quad (5)$$

It is known that there is an elliptical equation between the movement speed v and the displacement x of the blade. When $x = 0$, the blade's movement speed is at its maximum, and at this time, $v_{max} = r\omega$. When $x = \pm r$, that is, when a certain point on the cutting edge is in the extreme left or right position of the blade, the blade's movement speed is at its minimum and the acceleration is at its maximum. At this time, $v = 0$ and $v_{max} = r\omega^2$.

A schematic diagram of the cutter movement is shown in Figure 4.

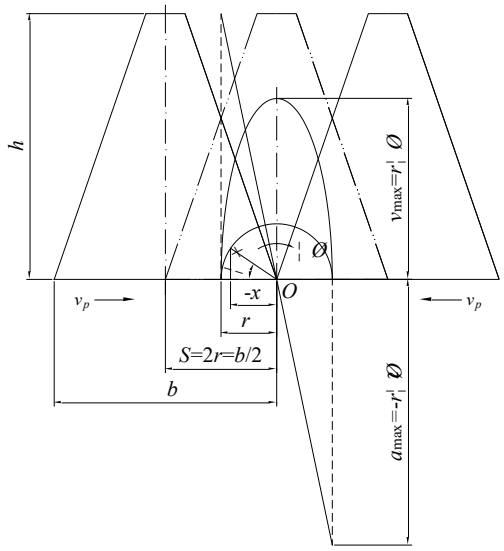

Figure 4. Schematic diagram of cutter movement.

The average cutting speed of the blade is generally expressed by the ratio of the cutting distance S to the time t taken to complete a cutting stroke, which is represented by v_p. The formula for v_p is:

$$v_p = \frac{nS}{30} \times 10^{-3} = \frac{rn}{15} \times 10^{-3} \quad (6)$$

Referring to the average cutting speed range of reciprocating blades for a ramie harvester [27], and taking its middle value, i.e., $v_p = 1.5$ m/s, the crank rotation speed n can be found to be 1181.1 r/min.

3.3. Bionic Blade Design

To facilitate the comparative study of the effects of different tooth pitch and tooth angle of bionic blades on cutting energy consumption, three-times the size of the biomimetic prototype (mouthparts palate of batocera horsfieldi) dimensions, i.e., 5.0 mm, 7.5 mm, and 10 mm, are used as tooth pitch sizes, and the mouthparts palate of batocera horsfieldi

is shown in Figure 5. The biomimetic principle involves using MATLAB image processing software to extract boundary point data of the arc-shaped contour of the mouthparts palate of batocera horsfieldi. After the extraction of the boundary points, curve fitting is performed on these points, and the fitted curve is then used as the design for the blade edge of the cutting blade [12]. For each tooth pitch, three tooth angles of 0°, 15°, and 30° are set for the blades. As a result, there are nine different combinations of blades with different tooth pitches and tooth angles. The different types of blades are shown in Figure 6, with their respective tooth pitch and tooth angle parameters listed in Table 1.

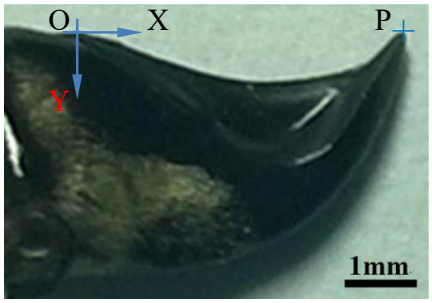

Figure 5. Mouthparts palate of batocera horsfieldi.

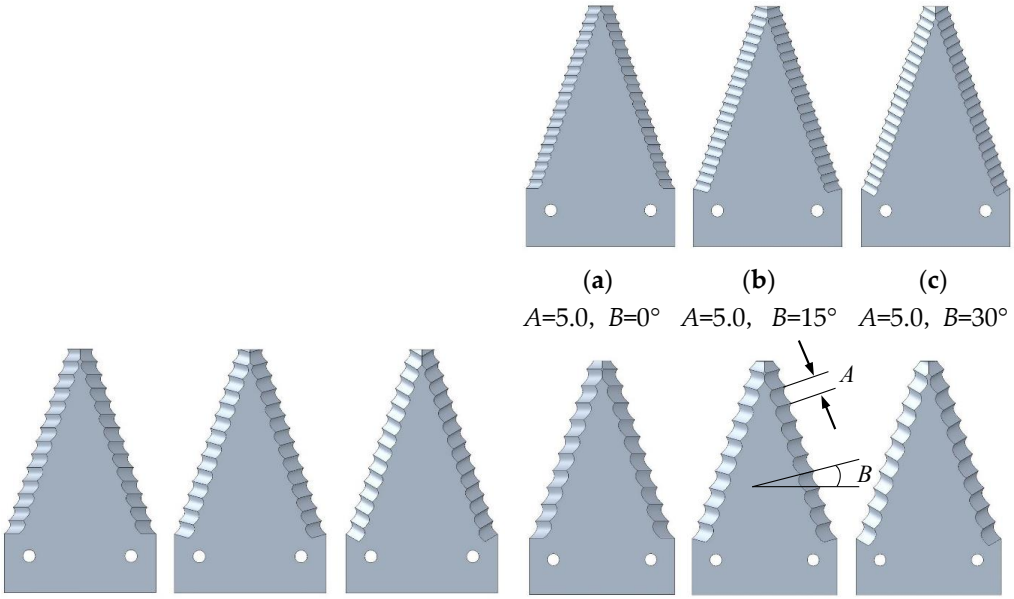

Figure 6. Bionic blades with different tooth pitches and tooth angles.

Table 1. Blade structure dimension parameter table.

Blade Code	Tooth Pitch *A*/mm	Tooth Angle *B*/°
a	5.0	0
b	5.0	15
c	5.0	30
d	7.5	0
e	7.5	15
f	7.5	30
g	10	0
h	10	15
i	10	30

Notes: *A* represents the tooth pitch; *B* represents the tooth angle.

4. Numerical Simulation and Analysis of Cutting Tests with Blade–Stalk Coupled Display of Dynamic Kinetics

4.1. Cutting Simulation Process and Determination of Material Parameters

The process of the numerical simulation of cutting experiments for the nonlinear display dynamics of the rigid–flexible coupling of the blade and hemp stalk is as follows: Based on the measured size of the industrial hemp stalk (stalk diameter of 18 mm), an industrial hemp stalk model is built in PTC Creo software. Different structural parameter bionic blade 3D models are designed and constructed, and the bionic blade and stalk models are assembled according to the actual cutting relationship. After determining the cutting relationship, the blade–hemp stalk 3D model is imported into the finite element analysis software ABAQUS through an intermediate format. According to the experimental plan, numerical simulation cutting experiments are conducted by defining material properties, assembling components, creating analysis steps, defining loads and boundary conditions, dividing the mesh, and submitting calculations. In defining the material properties of the model, the blade is set as a rigid body, while the stalk is set as a flexible body. According to measurements, the density of the stem is determined to be 9.5×10^{-9} t/mm^3, and the diameter is taken as the average value of the stem diameter, which is 18 mm. As the mechanical properties of industrial hemp stalks follow the transverse isotropy constitutive relationship, the engineering constants can be obtained from the literature [28]. Additionally, as the material characteristics of industrial hemp stalks are highly similar to wood, the anisotropic strength relationship of wood can be referenced to determine the anisotropic failure strength of industrial hemp stalks [29]. Therefore, the material property parameters of industrial hemp stalks based on the Hashin failure criterion can be obtained. The specific parameters are shown in Table 2.

Table 2. Mechanical property parameter table of stalk material of industrial hemp.

Mechanical parameter	E_X /MPa	E_Y /MPa	E_Z /MPa	G_{XY} /MPa	G_{XZ} /MPa	G_{YZ} /MPa	U_{XY}	U_{XZ}	U_{YZ}
Value	88	88	1743.50	33.85	31.99	31.99	0.3	0.02	0.02
Mechanical parameter	X_T /MPa	X_C /MPa	Y_T /MPa	Y_C /MPa	Z_T /MPa	Z_C /MPa	S_{XY} /MPa	S_{YZ} /MPa	S_{XZ} /MPa
Value	25	10	1	2	1	2	5	2	2

Note: E_X represents Young's modulus in X-direction; E_Y represents Young's modulus in Y-direction; E_Z represents Young's modulus in Z-direction; G_{XY} represents Shear modulus of plane XY; G_{XZ} represents Shear modulus of plane XZ; G_{YZ} represents Shear modulus of plane YZ; U_{XY} represents Poisson's ratio in plane XY; U_{XZ} represents Poisson's ratio in plane XZ; U_{YZ} represents Poisson's ratio in plane YZ; X_T represents Ultimate tensile stress in X-direction; X_C represents Ultimate compressive stress in X-direction; Y_T represents Ultimate tensile stress in Y-direction; Y_C represents Ultimate compressive stress in Y-direction; Z_T represents Ultimate tensile stress in Z-direction; Z_C represents Ultimate compressive stress in Z-direction; S_{XY} represents Ultimate shear stress in plane XY; S_{YZ} represents Ultimate shear stress in plane YZ; S_{XZ} represents Ultimate shear stress in plane XZ.

4.2. Experimental Design

Numerical simulation cutting experiments mainly investigated the effects of blade pitch, tooth angle, cutting speed ratio, and their interaction on blade cutting performance. In the case where the blade structure parameters are determined, it is necessary to determine the range of the speed ratio values. Referring to the speed ratio range of reciprocating cutters for stalk harvesters in the "Agricultural Machinery Design Manual", the speed ratio is set to be between 0.75 and 2 [26] (pp. 917). The experiment uses the three-factor three-level Box–Behnken response surface analysis method and cutting energy consumption as the index for orthogonal experimental design. The experimental factors and their level coding table are shown in Table 3.

The speed ratio coefficient is the ratio of the average cutting speed of the blade to the forward speed. As stated in Section 3.2, in this study, the value of v_p is 1500 mm/s. According to the formula for cutting speed and speed ratio $v_p = Cv_m$, the forward speed of

the blade under different speed ratios can be calculated. When $C = 0.75$, the blade's forward speed v_m is 2000 mm/s; when $C = 1.38$, v_m is 1090 mm/s; when $C = 2$, v_m is 750 mm/s.

Table 3. Factors and level coding table.

Levels	Factors		
	Tooth Pitch *A*/mm	**Tooth Angle *B*/°**	**Speed Ratio *C***
−1	5.0	0	0.75
0	7.5	15	1.38
1	10.0	30	2.00

4.3. Test Index

The bionic blade has the advantage of reducing resistance and consumption. This study focuses on the effect of different structural parameters and motion parameters of the bionic blade on the energy consumption of cutting, and the test index is the energy consumption of single stalk cutting.

Numerical simulations using ABAQUS to measure cutting energy consumption were carried out as follows: two sets, set-1 and set-2, were established for the driving constraints of the left and right blades, respectively. In the time history output of the analysis step, the reaction forces for these two sets were output separately. After submitting the job, the force–time curves and data of the two driving reference points could be obtained from the post-processing ODB file. The cutting energy consumption was calculated according to Formula (7).

$$W = \sum_{i}^{n} (F_{i1} + F_{i2}) \cdot v_P \cdot \Delta t \tag{7}$$

In the equation, W represents the cutting energy consumption in mJ; F_{i1} and $F_{i2,}$ respectively, represent the cutting reaction forces of the left and right blades at the i-th sampling point in N; v_p is the average cutting speed of the blade in mm/s; Δt is the sampling frequency interval time in s.

4.4. Experimental Results and Analysis

4.4.1. Regression Models and Analysis of Variance

The experimental design and analysis using Design-Expert software, experimental plan, and results are shown in Table 4. Taking experiment No. 13 as an example, the numerical simulation results, stubble cutting effect, and cutting force–time curve are shown in Figure 7.

Table 4. Experiment plan and results.

Test No.	Tooth Pitch *A*/mm	Tooth Angle *B*/°	Speed Ratio *C*	Cutting Energy *W*/mJ
1	−1	−1	0	6014.07
2	0	−1	1	4948.56
3	−1	0	1	4278.28
4	0	0	0	5531.58
5	1	1	0	5190.95
6	0	0	0	5531.58
7	0	0	0	5531.58
8	−1	0	−1	12,397.10
9	0	1	1	3972.02
10	1	0	1	3999.39
11	0	0	0	5531.58
12	−1	1	0	5424.18
13	1	−1	0	7201.73
14	0	−1	−1	16,033.50
15	0	0	0	5531.58
16	1	0	−1	11,869.80
17	0	1	−1	7343.06

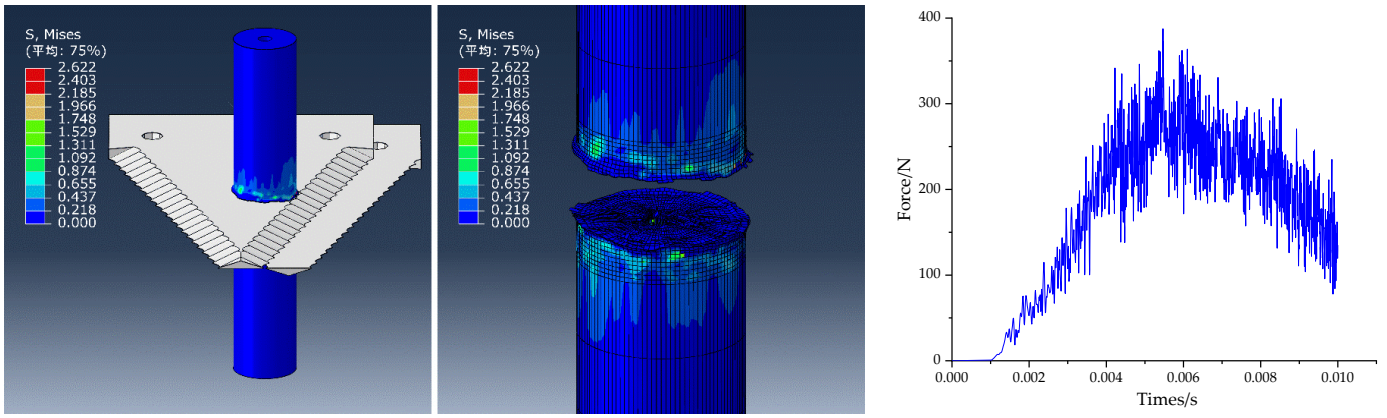

(**a**) A = 10 mm, B = 0°, C = 2 (**b**) Stubble cutting effect (**c**) Cutting force-time curve

Figure 7. Stalk cutting numerical simulation, stubble cutting effect, and cutting force–time curve. NOTE: " 平均" denotes average.

Through the Design-Expert, the response analysis of the experimental results was carried out using second-order regression, and the regression model equation for cutting energy consumption W was obtained as follows:

$$W = \begin{array}{l} 5531.58 + 18.53A - 1533.57B - 3805.77C - 355.22AB + \\ 62.10AC + 1928.24BC + 244.12A^2 + 182.03B^2 + 2360.44C^2 \end{array} \quad (8)$$

Further analysis of variance was conducted on the regression model of cutting energy consumption, and the results are shown in Table 5.

Table 5. Analysis of variance table for the regression model of cutting energy consumption.

Souces	Sum of Squares	*df*	Mean Square	*F*-Value	*p*-Value
Model	1.75×10^8	9	1.94×10^7	19.61	0.0004 **
A	2746.89	1	2746.89	0.0028	0.9594
B	1.88×10^7	1	1.88×10^7	19.02	0.0033 **
C	1.16×10^8	1	1.16×10^8	117.14	<0.0001 **
AB	5.05×10^5	1	5.05×10^5	0.5103	0.4981
AC	15,426.88	1	15,426.88	0.0156	0.9041
BC	1.49×10^7	1	1.49×10^7	15.04	0.0061 **
A^2	2.51×10^5	1	2.51×10^5	0.2537	0.6300
B^2	1.40×10^5	1	1.40×10^5	0.141	0.7184
C^2	2.35×10^7	1	2.35×10^7	23.72	0.0018 **
Residual	6.92×10^6	7	9.89×10^5		
Lack of Fit	6.92×10^6	3	2.31×10^6		
Cor Total	1.82×10^8	16			
R^2	0.9618				

Note: ** represents highly significant ($p < 0.01$).

The analysis of variance table above shows that the regression model for cutting energy consumption has a significance level p less than 0.01, indicating that the model has high significance. At the same time, the lack of a fit term in the model is not significant, and the fitting coefficient R^2 is 0.9618, indicating that the regression model obtained has a high degree of fit with the actual results, and the results are reliable. Therefore, the above model can be used to predict and analyze changes in cutting energy consumption.

Based on the above analysis of significance, for the cutting energy consumption indicator W, the factors of tooth angle B, speed ratio C, the interaction between B and C, and

C^2 have extremely significant impacts on the model, while other factors are not significant. The order of the main influences of each factor on cutting energy consumption is: $C > B > A$.

After eliminating the non-significant factors from the regression model of cutting energy consumption, the simplified regression model can be obtained as follows:

$$W = 5720.98 - 1533.57B - 3805.77C + 1928.24BC + 2384.12C^2 \quad (9)$$

4.4.2. Analysis of the Influence of Factor Interaction on Index

As can be seen from the variance analysis of the regression model mentioned above, the interaction between factors has a significant impact on the model. Therefore, the interaction between factors cannot be ignored. In this study, one factor was fixed at the middle level, and the interaction effects of the other two factors on the evaluation index were analyzed. Response surface plots were generated (as shown in Figure 8) to analyze the effects of the three factors, namely pitch, tooth angle, and speed ratio, on the cutting energy consumption index.

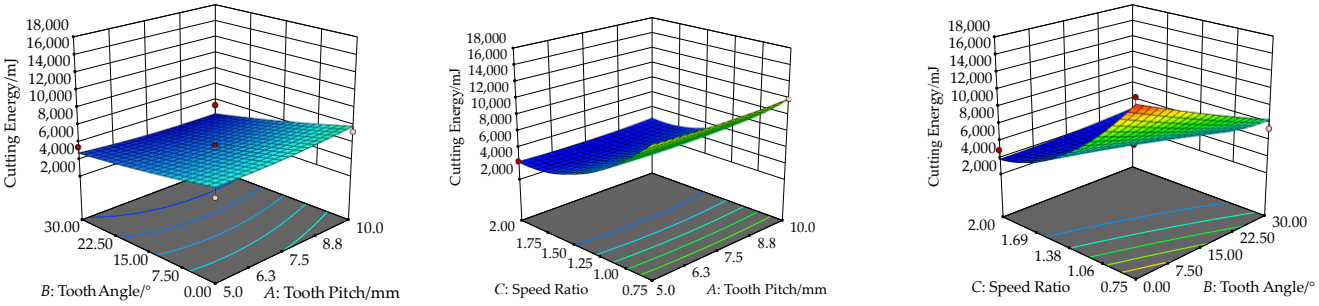

(**a**) $W = f(A, B, 1.38)$ (**b**) $W = f(A, 15, C)$ (**c**) $W = f(7.5, B, C)$

Figure 8. The interaction effect of two factors on cutting energy consumption.

Figure 8a shows the response surface of the interaction between tooth pitch A and tooth angle B on the cutting energy consumption when the speed ratio is at the middle level, i.e., C = 1.38. As can be seen from the figure, when the speed ratio is constant, the cutting energy consumption decreases as the tooth angle increases. Analysis shows that when the speed ratio is 1.38, the angle between the combined velocity vector of the blade's cutting speed and forward speed and the horizontal direction is 36° (calculated by arccot (1.38)). When the tooth angle B is 36°, the blade can cut into the stalk smoothly along the tooth groove, which is beneficial to reduce cutting resistance and energy consumption. Therefore, the closer the tooth angle is to 36 degrees, the lower the cutting energy consumption will be. This is shown in Figure 8a, where the cutting energy consumption decreases as the cutting rake angle increases. It can also be seen from Figure 8a that the change in cutting energy consumption with tooth pitch is not significant, indicating that cutting energy consumption is less affected by changes in tooth pitch.

Figure 8b shows the response surface plot of the interaction between the tooth pitch A and the speed ratio C on the cutting energy consumption when the tooth angle is set to the middle level of B = 15°. It can be seen from the plot that when the tooth angle is constant, the cutting energy consumption decreases rapidly with the increase in the speed ratio. Analysis indicates that to achieve the purpose of cutting with a parallel tooth system when the tooth angle is 15°, according to the calculation formula $\boldsymbol{C}$ = cot B, the speed ratio should be 3.73. Therefore, the cutting energy consumption in the plot decreases with the increase in the speed ratio. It can also be observed from the plot that the change in cutting energy consumption with tooth pitch is not significant, indicating that the variation in cutting energy consumption is less affected by the tooth pitch.

Figure 8c shows the response surface plot of the interaction between the tooth angle B and the speed ratio C on the cutting energy consumption when the tooth pitch is set to the middle level of A = 7.5 mm. It can be seen from the plot that when the tooth pitch is

constant, the cutting energy consumption decreases with the increase in the tooth angle and the speed ratio, indicating that the interaction between the tooth angle and the speed ratio has a significant impact on the cutting energy consumption index. The reason is similar to the analysis in Figure 8a,b.

4.5. Parameter Optimization and Experimental Verification

To further obtain the optimal combination of factor parameters corresponding to the lowest cutting energy consumption, it is necessary to comprehensively optimize the blade structure parameters and motion parameters. Design-Expert software was used for optimization, with the objective and constraint conditions as follows:

$$\begin{cases} \min W \\ s.t. \begin{cases} 5.0mm \leq A \leq 10.0mm \\ 0^\circ \leq B \leq 30^\circ \\ 0.75 \leq C \leq 2 \end{cases} \end{cases} \tag{10}$$

Via optimization, the optimal combination of blade structure and motion parameters was obtained, with a blade pitch of 6.61 mm, a tooth angle of 30°, and a speed ratio of 1.62 (corresponding to a horizontal motion speed of 1.5 m/s and a feed speed of 0.93 m/s). At this point, the cutting energy consumption was 3947.99 mJ.

To verify the optimization results, a three-dimensional blade model with a pitch of 6.61 mm and a tooth angle of 30° was constructed, imported into the finite element analysis ABAQUS software, and the cutting simulation experiment was conducted again with the cutting speed ratio set to 1.62. The cutting energy consumption under this parameter was calculated to be 3625.84 mJ, with an error of only 8.16% compared to the optimization result. The experiment showed that the optimization results were highly reliable, further validating the model's reliability.

5. Conclusions

(1) An analysis was carried out on the critical force condition for effective clamping of the stalk of the reciprocating double-acting cutting blade, and the analysis showed that the designed reciprocating bio-inspired cutting blade satisfies the conditions of effective clamping and non-slip. The motion analysis of the reciprocating double-acting cutting blade was carried out, and the analysis showed that compared with the single-acting cutting tool, the cutting stroke of the double-acting cutting blade can be reduced by half to complete a single cut. The elliptic equation relationship between the motion speed and displacement of the blade was also determined.

(2) In order to investigate the effects of different structural and motion parameters and their interactions on cutting energy consumption of bionic blades, a combination of bionic blades with different tooth pitch and tooth angle was designed. Numerical simulation experiments were conducted using numerical simulation techniques to cut industrial hemp stalk with the blades. Based on the experimental results, a regression optimization model for cutting energy consumption was established, and the optimal parameter combination was determined through optimization as follows: blade tooth pitch of 6.61 mm, tooth angle of 30°, and speed ratio of 1.62. The cutting energy consumption under these conditions was 3948.99 mJ. The accuracy of the numerical simulation model was verified through validation experiments. This study can provide reference for the development of an industrial hemp harvester cutter and the matching of motion parameters.

Author Contributions: Conceptualization, K.T. and A.J.; methodology, J.H. and B.Z.; software, J.H.; validation, C.S.; investigation, H.L.; writing—original draft preparation, K.T.; writing—review and editing, A.J. All authors have read and agreed to the published version of the manuscript.

Funding: This research was funded by the National Natural Science Foundation of China (Grant No. 52005274), the Key Laboratory of Modern Agricultural Equipment and Technology (Jiangsu University) (Grant No. MAET202103), the Earmarked Fund for Mordern Agro-industry Technology Research System (Grant No. CARS-16-E20), and the Agricultural Science and Technology Innovation Program of Chinese Academy of Agricultural Sciences (ASTIP, CAAS).

Institutional Review Board Statement: Not applicable.

Informed Consent Statement: Not applicable.

Data Availability Statement: Not applicable.

Conflicts of Interest: The authors declare no conflict of interest.

References

1. Zuk-Golaszewska, K.; Golaszewski, J. *Cannabis sativa* L.–cultivation and quality of raw material. *J. Elem.* **2018**, *23*, 971–984. [CrossRef]
2. Zhang, X.; Sun, Y.; Cao, K.; Jiang, Y.; Hang, C.; Zhao, Y.; Han, X.; Wang, X. Status and Prospect of Industrial Hemp Breeding in Heilongjiang Province. *Crops* **2019**, *35*, 15–19. [CrossRef]
3. Guo, L.; Wang, M.; Wang, D.; Li, Z.; Che, Y.; Zhang, H. Research progress and prospect of comprehensive utilization of industrial hemp. *Heilongjiang Agric. Sci.* **2014**, *8*, 132–134.
4. Kymäläinen, H.; Sjöberg, A. Flax and hemp fibres as raw materials for thermal insulations. *Build. Environ.* **2008**, *43*, 1261–1269. [CrossRef]
5. Lü, J.; Long, C.; Ma, L.; Liu, J.; He, H. Design and experiment on decorticator of hemp fresh stem. *Trans. CSAE* **2014**, *30*, 298–307. [CrossRef]
6. Sepe, R.; Bollino, F.; Boccarusso, L.; Caputo, F. Influence of chemical treatments on mechanical properties of hemp fiber reinforced composites. *Compos. Part B Eng.* **2018**, *133*, 210–217. [CrossRef]
7. Cao, K.; Wang, X.; Sun, Y.; Han, C.; Zhang, X.; Zhao, Y.; Jiang, Y.; Han, X.; Guo, Y. The research progress on the breeding of industrial hemp varieties in china. *Plant Fiber Sci. China* **2019**, *41*, 187–192.
8. Guo, R.; Chen, X.; Guo, H. Review on pharmacological effects of tetrahydrocannabinol and cannabidiol. *Nat. Prod. Res. Dev.* **2017**, *29*, 1449–1453. [CrossRef]
9. Pisanti, S.; Malfitano, A.; Ciaglia, E.; Lamberti, A.; Ranieri, R.; Cuomo, G.; Abate, M.; Faggiana, G.; Bifulco, M. Cannabidiol: State of the art and new challenges for therapeutic applications. *Pharmacol. Ther.* **2017**, *175*, 133–150. [CrossRef]
10. Available online: https://www.cn-healthcare.com/articlewm/20190430/content-1053495.html (accessed on 5 April 2022).
11. Huang, J.; Shen, C.; Li, X.; Tian, K.; Chen, Q.; Zhang, B. Design and tests of hemp harvester. *Int. Agric. Eng. J.* **2017**, *26*, 117–127.
12. Tian, K.; Li, X.; Shen, C.; Zhang, B.; Huang, J.; Wang, J.; Zhou, Y. Design and test of cutting blade of cannabis harvester based on longicorn bionic principle. *Trans. Chin. Soc. Agric. Eng.* **2017**, *33*, 56–61. [CrossRef]
13. Ahmadi, E.; Barikloo, H.; Kashfi, M. Viscoelastic finite element analysis of the dynamic behavior of apple under impact loading with regard to its different layers. *Comput. Electron. Agric.* **2016**, *121*, 1–11. [CrossRef]
14. Huang, H.; Wang, Y.; Tang, Y.; Zhao, F.; Kong, X. Finite element simulation of sugarcane cutting. *Trans. CSAE* **2011**, *27*, 161–166.
15. Qiu, M.; Meng, Y.; Li, Y.; Shen, X. Sugarcane stem cut quality investigated by finite element simulation and experiment. *Biosyst. Eng.* **2021**, *206*, 135–149. [CrossRef]
16. Yang, W.; Zhao, W.; Liu, Y.; Chen, Y.; Yang, J. Simulation of forces acting on the cutter blade surfaces and root system of sugarcane using FEM and SPH coupled method. *Comput. Electron. Agric.* **2021**, *180*, 105893. [CrossRef]
17. Xue, Z. Cutting Mechanical Characteristics and Simulation Analysis of Cassava Stalk. Ph.D. Dissertation, Huazhong Agriculture University, Wuhan, China, 2018.
18. Meng, Y.; Wei, J.; Wei, J.; Chen, H.; Cui, Y. An ANSYS/LS-Dyna simulation and experimental study of circular saw blade cutting system of mulberry cutting machine. *Comput. Electron. Agric.* **2019**, *157*, 38–48. [CrossRef]
19. Xie, L.; Wang, J.; Cheng, S.; Zeng, B.; Yang, Z. Optimization and finite element simulation of the chopping process for chopper sugarcane harvesting. *Biosyst. Eng.* **2018**, *175*, 16–26. [CrossRef]
20. Dun, G.; Yang, Y.; Li, H.; Yu, C.; Du, J.; Zhang, J.; Gao, Z. Working parameters optimization of soybean serration rotary cutter by ANSYS/LS—DYNA. *J. Henan Agric. Univ.* **2019**, *53*, 739–744.
21. Guo, Q.; Zhang, X.; Xu, Y.; Li, P.; Chen, C. Mechanism and simulation analysis of efficient cutting for tomato straw. *J. Agric. Mech. Res.* **2017**, *39*, 11–24. [CrossRef]
22. Zheng, C.; Zhao, J.; Zhang, J.; Zhang, R.; Li, F. Construction of finite element model of cotton pole and calibration of cutting parameters. *J. Agric. Mech. Res.* **2021**, *43*, 198–203. [CrossRef]

23. Wang, T.; Liu, Z.; Yan, X.; Mi, G.; Liu, S.; Chen, K.; Zhang, S.; Wang, X.; Zhang, S.; Wu, X. Finite Element Model Construction and Cutting Parameter Calibration of Wild Chrysanthemum Stem. *Agriculture* **2022**, *12*, 894. [CrossRef]
24. Liu, Z.; Wang, T.; Liu, S.; Yan, X.; Zhao, H.; Wu, X.; Zhang, S. Design and experimental study of a bionic blade for harvesting the wild chrysanthemum stem. *Agriculture* **2023**, *13*, 190. [CrossRef]
25. Xia, Z.; Yao, L.; Kan, J. The numerical simulation of rotating tool cutting soil and wood based on ANSYS/LS-DYNA. *For. Eng.* **2016**, *32*, 43–47. [CrossRef]
26. Chinese Academy of Agricultural Mechanization Science. *Agricultural Machinery Design Manual*, 1st ed.; China Agricultural Science and Technology Press: Beijing, China, 2007.
27. Shen, C.; Chen, Q.; Li, X.; Zhang, B.; Tian, K.; Huang, J. Design, analysis and test on cutting test bench of ramie stalk. *Int. Agric. Eng. J.* **2017**, *26*, 86–95.
28. Zhou, Y.; Li, X.; Shen, C.; Tian, K.; Zhang, B.; Huang, J. Experimental analysis on mechanical model of industrial hemp stalk. *Trans. CSAE* **2016**, *32*, 22–29. [CrossRef]
29. Available online: http://dec3.jlu.edu.cn/webcourse/T000185/T000199/files/bjjx/z8_2.html (accessed on 7 February 2023).